From growth surface to device interface: preserving metallic Fe under monolayer hexagonal boron nitride

Sabina Caneva,[1,#] Marie-Blandine Martin,[1,#] Lorenzo D'Arsié,[1] Adrianus I. Aria,[1] Hikmet Sezen,[2] Matteo Amati,[2] Luca Gregoratti,[2] Hisashi Sugime,[1] Santiago Esconjauregui,[1] John Robertson,[1] Stephan Hofmann,[1] and Robert S. Weatherup,[1,3,]*

[1]Department of Engineering, University of Cambridge, JJ Thomson Avenue, CB3 0FA, Cambridge, United Kingdom

[2]Elettra-Sincrotrone Trieste S.C.p.A., AREA Science Park, S.S. 14 km 163.5, 34149, Trieste, Italy

[3]Materials Sciences Division, Lawrence Berkeley National Laboratory, 1 Cyclotron Road, Berkeley California 94720, United States

* Corresponding author: rsw31@cam.ac.uk
[#]Equal contribution

ABSTRACT:

We investigate the interfacial chemistry between Fe catalyst foils and monolayer hexagonal boron nitride (h-BN) following chemical vapour deposition and during subsequent atmospheric exposure, using scanning electron microscopy, X-ray photoemission spectroscopy, and scanning photoelectron microscopy. We show that regions of the Fe surface covered by h-BN remain in a reduced state during exposure to moist air for ~40 hours at room temperature. This protection is attributed to the strong interfacial interaction between h-BN and Fe, which prevents the rapid intercalation of oxidizing species. Local Fe oxidation is observed on bare Fe regions and close to defects in the h-BN film (e.g. domain boundaries, wrinkles, and edges), which over the longer-term provide pathways for slow bulk oxidation of the Fe. We further confirm that the interface between h-BN and reduced Fe can be recovered by vacuum annealing at ~600 °C, although this is accompanied by the creation of defects within the h-BN film. We discuss the importance of these findings in the context of integrated manufacturing and transfer-free device integration of h-BN, particularly for technologically important applications where h-BN has potential as a tunnel barrier such as magnetic tunnel junctions.

Introduction

Hexagonal boron nitride (h-BN), the isostructural and electrically-insulating counterpart to graphene, is technologically promising not only as support for high mobility graphene and other 2D materials,[1] but given its low permeability to gases and thermo-chemical stability,[2–4] as an ultimately thin barrier layer for integrated electronics, photonics and spintronics.[5,6] A critical requirement for numerous emerging device concepts is that as well as the h-BN layers being of high crystalline quality, their interface to other materials must be clean and well controlled. While significant progress has been made in 2D material crystal growth,[7–9] particularly regarding scalable synthesis of h-BN films by chemical vapor deposition (CVD),[10–14] clean interfacing and scalable device integration remain major challenges. The latter typically involves transfer of the atomically thin h-BN layers away from the CVD growth substrate, and hence the choice of CVD catalyst/substrate and the related interfacial chemistry must be optimized towards ease of release of the h-BN.[15] Nevertheless, the potential for structural damage and contamination during transfer remains,[16] and avoiding this step offers a cleaner and simpler process flow that is more amenable to integrated manufacturing.

Transfer-free h-BN integration requires direct, conformal h-BN deposition onto a device relevant substrate. This has been demonstrated for instance for vertical magnetic tunnel junctions (MTJs), where the bottom ferromagnetic device layer acts as a catalytic growth substrate for h-BN CVD.[6] While previous literature focused mainly on the quality of as-grown h-BN, crucial for this approach is also that the device substrate is not negatively affected by the CVD process and that the resulting interface remains stable during further processing. The latter links to the question of how effectively 2D materials can protect different substrates. For graphene this has been investigated in detail and shown to relate to the strength of interaction between graphene and the

substrate.[17] Strongly interacting transition metals, such as Ni and Fe, with a significant degree of hybridization between the graphene π states and the d band states of the metal[18–20] prevent the rapid intercalation of oxidizing species at the graphene−metal interface and thus suppress oxidation and protect the metal surface. This protection can preserve clean, metallic interfaces which is a crucial requirement for effective spin injectors and the importance of this has been demonstrated for graphene-based MTJs.[21–23] Recent literature highlights that h-BN as a tunnel barrier may outperform widely used oxide barriers,[24,25] and when paired with a metallic ferromagnet can allow effective spin-filtering.[6,26–29] A tunnel magnetoresistance of up to 6% has already been demonstrated for a MTJ based on a single h-BN layer grown directly on the Fe electrode.[6] While high-quality h-BN CVD on Fe has been reported and it has been shown how boride and nitride formation in the Fe bulk can be avoided,[10,11] the nature and stability of an as-grown h-BN/Fe interface which is of utmost importance to device integration has not been studied in detail.

Here we use scanning electron microscopy (SEM), X-ray photoemission spectroscopy (XPS), and scanning photoelectron microscopy (SPEM) to systematically study the interfacial chemistry between Fe and h-BN after CVD and during subsequent atmospheric exposure. This model system has been chosen based on its particular relevance to MTJ device applications. Our SPEM data reveals that the Fe under the h-BN is protected from oxidation under ambient conditions for several days. The single-layer h-BN provides a low permeability barrier that restricts the access of oxidizing species to the metal surface, and the strong interaction between h-BN and Fe prevents the rapid intercalation of oxidizing species at the h-BN/Fe interface. However, Fe does not form a passivating oxide when exposed to moist air, therefore during continuing exposure the slow oxidation of the metal can proceed through the oxide layers formed in the vicinity of h-BN edges and defects. We further demonstrate that a h-BN/metallic-Fe interface can be recovered by vacuum annealing of a sample exposed to air for 7 days, with the reduction of the Fe confirmed

by XPS. We find that the general rationale for effective passivation by h-BN is consistent with a model developed for graphene,[17] and discuss the importance of our findings in the context of transfer-free h-BN device integration and MTJ applications where the protection demonstrated ensures a window for device processing in air and other oxidizing environments.

Results

We investigate the time-dependent oxidation behavior of polycrystalline Fe foils (100 μm thick) that have single-layer h-BN grown directly on their surface by CVD, and are subsequently exposed to atmospheric air at room temperature. All growths are performed in a customized CVD reactor (base pressure 10^{-6} mbar) with the Fe foils preannealed in NH_3 (4 mbar) at ~900 ºC prior to $B_3N_3H_6$ exposure at the same temperature. The preannealing enriches the Fe bulk with N, promoting the exclusive growth of single-layer h-BN on the catalyst surface and avoiding any Fe-boride formation.[11]

Figure 1 compares SEM images of discontinuous domains (a-c) and complete films (d-f) of single-layer h-BN on the Fe catalyst that have been exposed to air for different times following growth. The dark triangles in Figure 1a correspond to single-layer h-BN after 30 min of air exposure. After 1 day, thin bright veins can be observed crossing the domains (Figure 1b). We have previously shown by dark field transmission electron microscopy that the individual, triangular h-BN islands are single crystals,[11] therefore the bright veins are expected to relate to wrinkling of the h-BN caused by the thermal expansion mismatch with the underlying Fe, rather than domain boundaries in the h-BN.[30] After 7 days in air, the brighter regions are found to have grown at the expense of the darker regions within the domains. The inset shows a high magnification image of a small isolated h-BN domain which reveals a band of brighter contrast around the perimeter, indicating that the contrast change proceeds inwards from the edges. Figures 1d-f show the morphology of a complete single-

4

layer h-BN film (i.e. without bare Fe regions) after 30 min, 1 day and 7 days air exposure. The SEM contrast is again seen to evolve over time, from dark to bright. Following 30 min of air exposure, the h-BN related contrast is uniform and dark within each Fe grain. We note that the relatively minor grain-to-grain contrast variations of the Fe catalyst are related to the electron channeling contrast routinely observed for polycrystalline metal surfaces and do not reflect a variation in the thickness of the h-BN.[31] After 1 day, we again observe bright lines spreading across the surface and after 7 days the bright regions surround the few dark areas remaining. Figure S1 shows in more detail a representative area of the h-BN film after 1 day in air, where a network of brighter channels is apparent, from which the change in secondary electron contrast proceeds. Given the shapes and distribution of these channels, they are expected to correspond with the network of wrinkles and domain boundaries within the h-BN film.

Figure 1g shows in detail the edges and tips of several partially merged h-BN domains where different levels of contrast can be distinguished, labelled as regions 1, 2, and 3. It is interesting to note that the brightest regions (region 2, shaded red), whilst having lost their initial dark contrast (i.e. region 1), still bear the shape of the sharp h-BN domain edges, which can be distinguished from the areas of bare Fe (region 3). Figure 1h shows a false colored SEM image of a 'bow tie' h-BN domain structure, where two triangular domains have partially coalesced creating a domain boundary at the merging front. The domain edges and the domain-boundary region display a different contrast suggesting that the contrast changes proceed inwards from locations at which the atmosphere can more easily access the Fe foil, such as through edges and the defects present at boundaries (Figure 1i).[31,32]

We confirm that the change in SEM contrast is not indicative of a loss of h-BN material by transferring fresh h-BN domains (30 min air exposure) and aged domains (7 days air exposure)

onto SiO_2(300 nm)/Si wafers. The optical images in Figure 2a,b demonstrate that the triangular shapes and sizes of the h-BN domains are preserved, and are very similar to those of the domains grown on the catalyst (Figure 1a). The corresponding Raman spectra (Figure 2c) show very similar signatures for both samples, confirming that the h-BN is present on both and retains similar structural quality insofar as Raman spectroscopy is sensitive to this. Additionally, the XP B 1s and N 1s core level spectra for a non-transferred sample (i.e. h-BN/Fe) exposed to air for ~40 hours (Figure S2) exhibit a dominant B/N peak pair at 190.2/397.8 eV, which can be attributed to high quality monolayer h-BN.[11] This combined with the absence of any peak at ~193 eV in the B 1s core level, the typical position of boron oxide species,[33] indicates that the intrinsic chemical structure of the h-BN is not significantly altered by atmospheric air exposure. Further evidence that the h-BN is stable in air at room temperature over time is obtained without a transfer step, by vacuum annealing [~600 °C for 1 hour (< 10^{-5} mbar)] of a sample after 7 days of air exposure, as illustrated in Figure 3a-f. The behavior observed is schematically summarized in panels 3a-c, with the corresponding SEM images shown in panels 3d-f. At the onset of air exposure the h-BN domains on the metal surface show relatively homogeneous dark contrast (Figure 3a,d). With continued air exposure this contrast is gradually lost (Figure 3b,e). On vacuum annealing at ~600 °C the domains recover dark contrast similar to that observed for the fresh h-BN samples immediately after CVD (Figure 3c,f), further demonstrating that despite the changes in contrast, the h-BN remains intact. In situ XPS measurements of similar samples during vacuum annealing at ~600 °C show no emergence of a boron oxide related peak at ~193 eV nor any detectable oxygen species in the O 1s region, confirming the effective reduction of the Fe without oxidation of the h-BN (see Figure S4). However, XPS measurements after a further air exposure, reveal some oxidation of the h-BN films as manifested by the appearance of a boron oxide peak at ~193 eV. This therefore indicates that the annealing process has led to some degradation of the h-BN, with

6

defects formed which are then oxidized on air exposure.

Figure 4a,b shows XP spectra of the Fe $2p_{3/2}$ core level for a complete h-BN film and discontinuous domains respectively as a function of air exposure time. After 1 day in air, the spectra for the complete film displays a dominant metallic peak at 706.7 eV (Fe$_M$) and negligible oxide-related components, indicating that the Fe is well reduced. After 7 days, the Fe is still mainly in the reduced state, however a small peak at the oxide position emerges above the noise level, at ~711 eV (Fe$_{OX}$), which is indicative of slight oxidation. This behaviour is in strong contrast to bare Fe, where significant oxidation of the surface is observed following air exposures of just one hour, but is in excellent agreement with our previous studies on air-exposed graphene-coated Fe substrates, where gradual oxidation of the metal is observed.[17] For discontinuous h-BN domains (Figure 4b) spectral components related to both metallic and oxidized Fe are observed following 1 day of air exposure. The metallic peak dominates over the oxide-related peak, indicating the Fe remains predominantly reduced, consistent with only the exposed Fe regions oxidizing whilst the h-BN covered regions remain reduced. However, after 7 days, the extent of Fe oxidation is significantly increased, as revealed by the greater intensity of the oxide components relative to the metal peak.

Figure 5a shows a SPEM map of h-BN domains grown on Fe foil (same growth conditions as in Figure 1a) acquired for the B 1s core level energy, following exposure to atmospheric air for ~40 hours at room temperature. The schematic in the inset indicates that the light grey triangles correspond to h-BN domains while the surrounding dark areas are the bare Fe surface, as subsequently confirmed by the maps in Figure 5c,d. The XP spectra of the Fe $2p_{3/2}$ core level were acquired on the bare Fe (region A) and on several h-BN domains (region B), as shown in Figure 5b. The change in spectral components present in these two regions indicates a distinct difference in the oxidation state of the Fe between the h-BN covered regions and bare Fe.

7

The peaks from region A are attributable to Fe oxide/oxyhydroxide species (Fe$_{OX}$),[34] whereas the peaks from region B corresponds to metallic Fe (Fe$_M$). Figures 5c-e show elemental maps of the edge and tips of several h-BN domains and the neighboring bare Fe surface using the B 1s and N 1s peak intensities, and the intensity ratio between metal and oxide components in the Fe 2$p_{3/2}$ region respectively. In the B 1s and N 1s maps, the right hand side of the image appears brighter, indicating a higher signal originating from this area, which confirms h-BN coverage of this region. We note that a Fe grain boundary can be seen crossing slightly diagonally from the top to the bottom of Figures 5c,d across several h-BN domains, which is apparent due to topographic changes in the XP signal. Figure 5e, which depicts a map of the ratio between metal and oxide components of the Fe 2$p_{3/2}$ core level, is a background-corrected chemical map (see methods) where the intensity changes generated by the topography of the sample are intrinsically removed, thus revealing only chemical data. The brightest contrast, that is the predominantly metallic Fe, corresponds to the h-BN covered region on the right hand side, confirming that oxidation protection arises from the h-BN coverage. The fact that the contrast level is also maintained across the Fe grain boundary indicates that the extent of protection afforded by the h-BN layer is maintained in spite of the topography of the underlying substrate. Where the h-BN is absent on the left hand side of Figure 1e, the signal is less bright confirming that the uncovered Fe is predominantly oxidized. B 1s and N 1s chemical maps with the topographic component removed are shown in Figure S3.

Discussion

The changes in SEM contrast observed in Figure 1 may at first sight appear to correspond to degradation of the h-BN in air, however our XPS and SPEM data confirm that they instead relate to the gradual oxidation of the Fe substrate beneath the h-BN. Similar contrast changes are observed for graphene on weakly-interacting metals due to the intercalation of oxidizing species which alter the charge-transfer doping from the underlying substrate and thus the

work function of the graphene, without otherwise significantly disturbing its bandstructure.[17,35] In the case of h-BN on Fe, intercalation is suppressed due to the strong interaction between h-BN and the substrate, but as our XPS measurements here show, oxidation can still proceed through the Fe bulk. The changes in SEM contrast observed for h-BN covered regions are therefore attributable to the different secondary electron yields of oxidized and metallic Fe, as well as possible variations in work function associated with changes in hybridization between the h-BN and substrate (i.e. alteration of the h-BN band structure[36–38]) as the substrate oxidizes. The changes in the SEM contrast from dark to light with continuing air exposure are thus indicative of oxidation of the underlying metal. We can therefore assign the different contrast levels in Figure 1g to h-BN covered metallic Fe (h-BN/Fe$_M$) in region 1, h-BN covered oxidized Fe (h-BN/Fe$_{OX}$) in region 2 and bare Fe in region 3. The contrast changes apparent in Figure 1 thus correspond to Fe oxidation proceeding via domain edges, domain-boundary defects and wrinkles of the h-BN layer, which serve as pathways for oxidizing species to reach the Fe surface during atmospheric air exposure. Given the detrimental effect of wrinkles on the passivation behavior of 2D films, we envisage that future work could be aimed at minimizing wrinkle formation during CVD growth by, for instance, varying the thickness of the catalyst, as has been reported for graphene CVD.[39]

The XPS spectra shown in Figure 4, acquired using a X-ray spot size of ~150 μm, further confirm that oxidation proceeds through these pathways. In the case of the continuous h-BN film, the region probed is fully covered with h-BN and Figure 4a clearly confirms that the Fe is protected from any substantial oxidation over the course of 1 day and that even after 7 days of air exposure, the level of oxidation remains relatively low. For the discontinuous domains, the level of oxidation after 1 day is significantly increased, showing that the degree of protection depends on the extent of h-BN coverage. Furthermore the increase in oxidation

after 7 days is much more pronounced than for the continuous h-BN film, indicating that the increased prevalence of "open edges" allows oxidation to proceeds more readily. However, as the XPS spot includes both covered and uncovered regions, we note that Figure 4b does not necessarily imply that the discontinuous h-BN domains do not locally protect the Fe. This point is clarified by Figure 5 where spatially resolved XP spectra of the Fe $2p_{3/2}$ reveal that in the short term (~40 hours), significant oxidation (Fe_{OX}) is only observed in regions of the surface that are not covered by h-BN, with the h-BN covered regions remaining reduced (Fe_M).

The observed oxidation behavior can be understood in the context of the model recently introduced by Weatherup et al.[5] to explain the behavior of different graphene/metal couples as a function of their interfacial interaction strength and the nature of the oxide formed by the substrate. Here we extend this model to h-BN on Fe as summarized in Figure 3, highlighting its general applicability to other 2D materials. During initial exposure to atmospheric air at room temperature, h-BN grown on Fe provides a low permeability barrier that restricts the access of oxidizing species to the underlying metal. Furthermore, the strong interaction between h-BN and Fe prevents intercalation of oxidizing species at the h-BN metal interface. Rapid oxidation thus only occurs at uncovered regions or close to intrinsic defects in the h-BN film (e.g. vacancies, grain boundaries) that provide pathways for oxidizing species to reach the substrate (shaded red, Figure 3a), while the areas with pristine h-BN coverage remain reduced (Fe_M). As discussed further below, Fe does not form a passivating oxide when exposed to moist air.[40] Therefore during continuing exposure (days) oxidation can proceed through the oxide layers formed in the vicinity of h-BN edges and defects (expanding Fe_{OX} region underneath the strongly-coupled h-BN in Figure 3b), with the Fe eventually becoming oxidized throughout. This process can be subsequently reversed by vacuum annealing which leads to reduction of the Fe layer (Figure 3c). Our results herein for h-BN and previous work

on graphene[17] emphasize the importance of interfacial interaction strength in how effectively a 2D material protects a substrates. We therefore expect the development of methods to engineer this interfacial interaction strength, through techniques such as alloying or interfacial intercalation, to be a promising avenue for protecting material surfaces whilst retaining their functional (e.g. catalytic,[41,42] plasmonic,[43] spin-filtering[6,21–23]) properties.

In this work we employ polycrystalline Fe foils comprising multiple crystal orientations and note that the h-BN domains readily grow across Fe grain boundaries. Furthermore, Fe can undergo a range of phase transformations and reactions with boron and nitrogen during the CVD process including upon cooling.[11] The nature of the edge bonding and any epitaxial relationship will therefore vary across different Fe grains, within h-BN domains, and at different stages of the growth process, precluding here a simple explanation of local oxidation behavior based on interlayer distance, epitaxial relationship or edge bonding state. The formation of wrinkles in the h-BN layer, which provide pathways between the h-BN and Fe for more rapid surface oxidation, is also likely to be impacted by the complex phase behavior that the Fe surfaces undergo. Interestingly, we note that the general oxidation behavior of regions away from wrinkles appears similar across multiple h-BN domains on several samples. This indicates that the first-order picture of oxidation behavior we develop, based on a strong Fe and h-BN hybridization preventing rapid intercalation of oxidizing species, is relevant across such complex polycrystalline surfaces.

Previous XPS studies on the behavior of polycrystalline Fe surfaces exposed to either oxygen or water vapor have elucidated the various stages of the oxidation mechanisms.[44,45] In both cases, current interpretation suggests a thin surface oxide initially forms by a place-exchange mechanism, and then growth of the oxide proceeds by electric-field driven diffusion of ions through vacancies, interstitial sites and grain boundaries. As the oxide thickness increases the electric field strength reduces limiting the oxide thickness to several nanometers. A slower

11

rate of oxide thickening is observed for H_2O compared to O_2, which is attributable to the presence of hydrogen which restricts ion diffusion and occupies surface sites that would otherwise be available for further H_2O adsorption.[45] When bare Fe is instead exposed to moist air containing both O_2 and H_2O, a hydrated oxide forms as a loose deposit that provides very limited protection against further oxidation.[40] Therefore whilst an h-BN overlayer prevents oxidation of the Fe surface beneath for several days by acting as an impermeable barrier, the Fe does not form an effective passivating oxide that can 'plug' regions near h-BN defects and edges and therefore oxidation proceeds through the Fe bulk over the longer-term.

In contrast to graphene-covered metals the h-BN is not expected to promote galvanic corrosion despite the presence of moist air, as its insulating nature prevents electron conduction to the oxygen atoms. However, the presence of h-BN edges and the confined space between the metal and h-BN may potentially influence the passivation behavior. For metal substrates including Pt, Rh, and Ru confinement of molecules beneath a 2D layer may enhance metal-catalyzed reactions by modifying the adsorbate−metal interaction and potentially causing reconstruction of the metal surface.[46–48] In our case, however, the strong interaction between Fe and h-BN suppresses intercalation of molecules, and we therefore suggest that any change in the reactivity of the Fe caused by the h-BN is likely to only occur locally at the h-BN wrinkles or grain boundaries, which constitute a small proportion of the total surface.

A key consideration in selecting a passivating layer, is its stability in its intended operating environment. For certain 2D materials, including MoS_2, WS_2 and black phosphorous, significant structural degradation has been reported under atmospheric conditions at room temperature.[49–51] However, h-BN is expected to exhibit excellent stability under atmospheric conditions, and indeed the optical images and Raman spectra we obtain (Figure 2) confirm that the h-BN on Fe does not undergo significant deterioration of its structural quality during

room temperature air exposure. We further exclude significant defect formation within the domains after room temperature air exposure based on the absence of any component in the XP spectra at ~193 eV (figure S2), which is typically attributed to boron oxide species[33,52] whose formation has been linked to the loss of N atoms from the h-BN lattice.[53] This excellent stability in air is also evidenced by the recovery of the initial, dark SEM contrast in h-BN covered regions after vacuum annealing (Figure 3f). The reduction of the underlying Fe that occurs during this process (as confirmed by XPS in figure S4), is achieved without accompanying structural damage being detected with SEM. In contrast, SEM following vacuum annealing of air-exposed graphene on Cu and h-BN on Cu reveals that significant etching of the 2D materials occurs. In situ XPS confirms that this happen at temperature by carbothermal reduction of the oxidized Cu substrate[35] and formation of volatile boron oxides, for the graphene and h-BN respectively, with the extent of damage linked to the amount of substrate oxidation and oxygen species present at the interface as well as the catalytic nature of the substrate (including crystal orientation).[52] On Cu, which exhibits a weak interaction with graphene and h-BN, rapid decoupling on air exposure allows oxidizing species to readily access the Cu and thus a relatively large oxygen reservoir for etching can develop. Our in situ measurements on Fe herein show no detectable boron oxide species (either in the B 1s or O 1s spectra) during annealing (Figure S4). Nevertheless, we do find that annealing induces some minor degradation of the h-BN, as evidenced by the appearance of a boron oxide peak in the B 1s spectrum following subsequent air exposure (Figure S4c) which we attribute to the decoration of defects induced in the h-BN during annealing. This indicates that catalytic etching of h-BN on Fe can still occur, but that this is relatively minor as only a small oxygen reservoir is formed over the timescales considered here, thanks to the strong interfacial interaction that suppresses Fe oxidation. However, this does call into question the viability of using thin h-BN layers as oxidation-resistant coatings under high-temperature conditions,[3] as

the potential for catalytic degradation of the h-BN by the substrate it is protecting must be carefully considered. We emphasize that the post-annealed Fe surface remains reduced during subsequent exposure to air, as shown in Figure 3f, and hence demonstrate that protection can be re-established through this treatment.

Our results demonstrate that single-layer h-BN can protect Fe from oxidation for several days without undergoing any significant degradation. While the protection afforded is not superior to that of graphene-covered Ni substrates which remain reduced for >18 months,[17] it is comparable to that of graphene on Fe surfaces with the added advantage that the insulating h-BN avoids the formation of a galvanic couple[54–56] which may otherwise accelerate corrosion of the underlying metal, as observed for graphene on Cu.[57] Furthermore, while bare Fe oxidizes almost immediately upon air exposure, we show that h-BN/Fe stacks offer a promising route for maintaining a reduced Fe surface when fabricating devices, where short air exposures between process steps including lithography, development and lift off, as well as transfer of additional h-BN layers in air, can simplify fabrication or where oxidizing processing steps are required (e.g. atomic-layer/pulsed-laser deposition of oxides,[22,58] oxygen plasma to remove organic contaminants). Indeed, such integrated processing has been demonstrated by the incorporation of h-BN grown by CVD on Fe electrodes into functional magnetic tunnel junctions,[6] where the h-BN serves both as a tunnel barrier and as an oxidation barrier for the Fe. Furthermore, the thermo-chemical stability of h-BN is expected to be particularly advantageous in aggressive processing environments, where other 2D materials would be damaged or removed.

Conclusion

In summary, we have shown that single-layer h-BN grown on polycrystalline Fe foils protects the covered Fe surface from oxidation during exposure to moist air for more than 40 hours at

14

room temperature, whilst uncovered Fe regions become oxidized. This protection is attributed to the strong interaction between the h-BN and Fe substrate which suppresses the rapid intercalation of oxidizing species along the interface between them. Over the longer-term, slow bulk oxidation of the Fe proceeds through the oxide layers formed in the vicinity of h-BN edges and defects, with the Fe eventually becoming oxidized throughout. The behavior observed is in excellent agreement with the model developed by Weatherup *et al.* to explain the passivation behavior of different graphene-covered metals,[17] demonstrating that this general rationale can be extended to other 2D materials. We confirm that the h-BN remains stable during air exposure, with no oxidation of the h-BN detected. On post-annealing in vacuum, the Fe can be fully reduced whilst the h-BN remains largely intact, confirming that even after extended air exposures the reduced h-BN/Fe stack can be recovered. This annealing is found to induce some defects in the h-BN due to catalytic etching by the Fe support, highlighting that the thermal stability of the h-BN can be affected by the substrate on which it sits. Our results highlight the potential of h-BN films for preserving the surface of ferromagnetic electrodes in a reduced state during processing under oxidizing environments which is particularly relevant to the transfer-free integration of h-BN in devices such as MTJs.

Methods

h-BN growth. CVD growth is performed using a recipe previously reported.[11] As-received Fe foil (0.1 mm, Alfa Aesar, 99.99% purity) is used as the catalyst substrate for the growth of h-BN domains and films in a customized Aixtron BM3 cold-wall reactor (base pressure $<10^{-6}$ mbar), using $B_3N_3H_6$ (6×10^{-4} mbar, FluoroChem, >97% purity) as the precursor at ~900 ºC. The samples are typically heated in 4 mbar of NH_3 at 100 ºC/min up to 750 ºC and then at 50 ºC/min up to ~900 ºC. Immediately after reaching ~900 ºC, the NH_3 is removed. $B_3N_3H_6$ is dosed into the chamber through a leak valve (from a liquid reservoir) and after growth the

$B_3N_3H_6$ leak valve is closed and the heater is turned off. Samples are cooled in vacuum by immediately switching off the heater (cooling rate ~300 ºC/min down to ~500 ºC, after which it slows down further).

Transfer. For optical microscopy and Raman spectroscopy we transfer the h-BN using an electrochemical bubbling method.[59] We perform the transfer by spin coating a support layer of polymethylmethacrylate (PMMA) onto the sample surface. The sample is placed in a NaOH bath (1M) and a negative voltage is applied relative to a Pt electrode, which causes H_2 bubbles to evolve at the h-BN/Fe interface, detaching the film from the substrate. The PMMA/h-BN film is rinsed in deionized water and scooped onto a SiO_2(300 nm)/Si wafer where it is left to dry. The PMMA is removed by immersing the sample in acetone for ~12 hours, followed by a rinse in IPA. The samples are annealed in vacuum at 500 ºC for 1 hour to remove residual PMMA.[16]

Characterization. For the ex situ characterization of the h-BN on the catalyst we use scanning electron microscopy (SEM, Zeiss SigmaVP, 2kV). Optical images are acquired using a Nikon eclipse ME600L microscope and Raman measurements are performed with a Renishaw In-Via microscope using a 100× objective and 532 nm laser excitation.

XP spectra of the $Fe2p_{3/2}$ core level were collected using a Thermo Scientific ESCALAB 250Xi at an operating pressure $<10^{-10}$ mbar. X-ray illumination was provided by a micro-focused, monochromated Al Kα source with a photon energy of 1486.6 eV and a spot size of ~150 μm diameter. The emitted photoelectrons were collected by a hemispherical energy analyzer with a spectral resolution of ±0.1 eV.

The X-ray photoelectron microscopy/micro-spectroscopy measurements were carried out with the SPEM instrument at the Escamicroscopy beamline of the Elettra synchrotron facility (Trieste, Italy). The X-ray beam was focused to ~130 nm by a Fresnel zone plate and an order sorting aperture. For both imaging and submicron spectroscopy a SPECS-PHOIBOS 100

hemispherical electron energy analyzer with an in-house customized multichannel plate detector was used. A photon energy of 1102 eV was employed. The SPEM imaging mode can map the photoelectrons emitted within a selected kinetic energy window by scanning the specimen with respect to the X-ray beam. The SPEM micro-spectroscopy mode is the typical energy scanning mode employed in any standard XPS system, using a 130 nm X-ray spot size. All binding energies are referenced to measured Fermi edges.

ACKNOWLEDGEMENTS

ASSOCIATED CONTENT

Supporting Information

SEM image of Fe oxidation along specific channels in the h-BN film; XP spectra of the B 1*s* core level; SPEM chemical maps acquired with the B 1*s*, N 1*s* core level energies; XPS data showing the reduction of an Fe foil during annealing in vacuum.

REFERENCES

(1)   Dean, C. R.; Young, A. F.; Meric, I.; Lee, C.; Wang, L.; Sorgenfrei, S.; Watanabe, K.; Taniguchi, T.; Kim, P.; Shepard, K. L.; Hone, J. Boron Nitride Substrates for High-Quality Graphene Electronics. *Nat. Nanotechnol.* **2010**, *5*, 722–726.

(2)   Bunch, J. S.; Verbridge, S. S.; Alden, J. S.; van der Zande, A. M.; Parpia, J. M.; Craighead, H. G.; McEuen, P. L. Impermeable Atomic Membranes from Graphene Sheets. *Nano Lett.* **2008**, *8*, 2458–2462.

(3)   Liu, Z.; Gong, Y.; Zhou, W.; Ma, L.; Yu, J.; Idrobo, J. C.; Jung, J.; MacDonald, A. H.; Vajtai, R.; Lou, J.; Ajayan, P. M. Ultrathin High-Temperature Oxidation-Resistant Coatings of Hexagonal Boron Nitride. *Nat. Commun.* **2013**, *4*, 2541.

(4)   Li, L. H.; Cervenka, J.; Watanabe, K.; Taniguchi, T.; Chen, Y. Strong Oxidation Resistance of Atomically Thin Boron Nitride Nanosheets. *ACS Nano* **2014**, *8*, 1457–1462.

(5)   Ferrari, A. C.; Bonaccorso, F.; Falko, V.; Novoselov, K. S.; Roche, S.; Bøggild, P.; Borini, S.; Koppens, F.; Palermo, V.; Pugno, N.; Garrido, J. a; Sordan, R.; Bianco, A.; Ballerini, L.; Prato, M.; Lidorikis, E.; Kivioja, J.; Marinelli, C.; Ryhänen, T.; Morpurgo, A.; Coleman, J. N.; Nicolosi, V.; Colombo, L.; Fert, A.; Garcia-Hernandez, M.; Bachtold, A.; Schneider, G. F.; Guinea, F.; Dekker, C.; Barbone, M.; Galiotis, C.; Grigorenko, A.; Konstantatos, G.; Kis, A.; Katsnelson, M.; Beenakker, C. W. J.; Vandersypen, L.; Loiseau, A.; Morandi, V.; Neumaier, D.; Treossi, E.; Pellegrini, V.; Polini, M.; Tredicucci, A.; Williams, G. M.; Hong, B. H.; Ahn, J. H.; Kim, J. M.; Zirath, H.; van Wees, B. J.; van der Zant, H.; Occhipinti, L.; Di Matteo, A.; Kinloch, I. a; Seyller, T.; Quesnel, E.; Feng, X.; Teo, K.; Rupesinghe, N.; Hakonen, P.; Neil, S. R. T.; Tannock, Q.; Löfwander, T.; Kinaret, J. Science and Technology Roadmap for Graphene, Related Two-Dimensional Crystals, and Hybrid Systems. *Nanoscale* **2015**, *7*, 4598–4810.

(6)   Piquemal-Banci, M.; Galceran, R.; Caneva, S.; Martin, M.-B.; Weatherup, R. S.; Kidambi, P. R.; Bouzehouane, K.; Xavier, S.; Anane, A.; Petroff, F.; Fert, A.; Robertson, J.; Hofmann, S.; Dlubak, B.; Seneor, P. Magnetic Tunnel Junctions with Monolayer Hexagonal Boron Nitride Tunnel Barriers. *Appl. Phys. Lett.* **2016**, *108* (10), 102404.

(7)   Hao, Y.; Bharathi, M.; Wang, L.; Liu, Y.; Chen, H.; Nie, S.; Wang, X.; Chou, H.; Tan, C.; Fallahazad, B.; Ramanarayan, H.; Magnuson, C. W.; Tutuc, E.; Yakobson, B. I.; McCarty, K. F.; Zhang, Y.-W.; Kim, P.; Hone, J.; Colombo, L.; Ruoff, R. S. The Role of Surface Oxygen in the Growth of Large Single-Crystal Graphene on Copper. *Science* **2013**, *342*, 720–723.

(8)   Weatherup, R. S.; Shahani, A. J.; Wang, Z.-J.; Mingard, K.; Pollard, A. J.; Willinger, M. G.; Schloegl, R.; Voorhees, P. W.; Hofmann, S. In Situ Graphene Growth Dynamics on Polycrystalline Catalyst Foils. *Nano Lett.* **2016**, *16*, 6196–6206.

(9)   Nagashima, A.; Tejima, N.; Oshima, C. Electronic States of the Pristine and Alkali-Metal-Intercalated Monolayer graphite/Ni(111) Systems. *Phys. Rev. B* **1994**, *50*, 17487–17495.

(10)   Caneva, S.; Weatherup, R. S.; Bayer, B.; Brennan, B.; Spencer, S. J.; Mingard, K.; Cabrero-Vilatela, A.; Baehtz, C.; Pollard, A. J.; Hofmann, S. Nucleation Control for

Large, Single Crystalline Domains of Monolayer Hexagonal Boron Nitride via Si-Doped Fe Catalysts. *Nano Lett.* **2015**, *15*, 1867–1875.

(11) Caneva, S.; Weatherup, R. S.; Bayer, B. C.; Blume, R.; Cabrero-Vilatela, A.; Braeuninger-Weimer, P.; Martin, M.-B.; Wang, R.; Baehtz, C.; Schlögl, R.; Meyer, J. C.; Hofmann, S. Controlling Catalyst Bulk Reservoir Effects for Monolayer Hexagonal Boron Nitride CVD. *Nano Lett.* **2016**, *16*, 1250–1261.

(12) Lu, G.; Wu, T.; Yuan, Q.; Wang, H.; Wang, H.; Ding, F.; Xie, X.; Jiang, M. Synthesis of Large Single-Crystal Hexagonal Boron Nitride Grains on Cu-Ni Alloy. *Nat. Commun.* **2015**, *6*, 6160.

(13) Stehle, Y.; Meyer, H. M.; Unocic, R. R.; Kidder, M.; Polizos, G.; Datskos, P. G.; Jackson, R.; Smirnov, S. N.; Vlassiouk, I. V. Synthesis of Hexagonal Boron Nitride Monolayer: Control of Nucleation and Crystal Morphology. *Chem. Mater.* **2015**, *27* (23), 8041–8047.

(14) Oshima, C.; Nagashima, A. Ultra-Thin Epitaxial Films of Graphite and Hexagonal Boron Nitride on Solid Surfaces. *J. Phys. Condens. Matter* **1997**, *9*, 1–20.

(15) Wang, R.; Whelan, P. R.; Braeuninger-Weimer, P.; Tappertzhofen, S.; Alexander-Webber, J. A.; Van-Veldhoven, Z. A.; Kidambi, P. R.; Jessen, B. S.; Booth, T. J.; Boggild, P.; Hofmann, S. Catalyst Interface Engineering for Improved 2D Film Lift-Off and Transfer. *ACS Appl. Mater. Interfaces* **2016**, *8*, 33072.

(16) Kratzer, M.; Bayer, B. C.; Kidambi, P. R.; Matković, A.; Gajić, R.; Cabrero-, A.; Weatherup, R. S.; Hofmann, S.; Teichert, C. Effects of Polymethylmethacrylate-Transfer Residues on the Growth of Organic Semiconductor Molecules on Chemical Vapor Deposited Graphene. *Appl. Phys. Lett.* **2015**, *106*, 103101.

(17) Weatherup, R. S.; D'Arsié, L.; Cabrero-Vilatela, A.; Caneva, S.; Blume, R.; Robertson, J.; Schlögl, R.; Hofmann, S. Long-Term Passivation of Strongly Interacting Metals with Single-Layer Graphene. *J. Am. Chem. Soc.* **2015**, *137*, 14358–14366.

(18) Dedkov, Y. S.; Fonin, M.; Rüdiger, U.; Laubschat, C. Graphene-Protected Iron Layer on Ni(111). *Appl. Phys. Lett.* **2008**, *93*, 22509.

(19) Dahal, A.; Batzill, M. Graphene-Nickel Interfaces: A Review. *Nanoscale* **2014**, *6*, 2548–2562.

(20) Weatherup, R. S.; Amara, H.; Blume, R.; Dlubak, B.; Bayer, B. C.; Diarra, M.; Bahri, M.; Cabrero-vilatela, A.; Caneva, S.; Kidambi, P. R.; Martin, M.; Deranlot, C.; Seneor, P.; Schloegl, R.; Bichara, C.; Hofmann, S.; Ducastelle, F.; Bichara, C.; Hofmann, S. Interdependency of Subsurface Carbon Distribution and Graphene-Catalyst Interactions. *J. Am. Chem. Soc.* **2014**, *136*, 13698–13708.

(21) Dlubak, B.; Martin, M.-B.; Weatherup, R. S.; Yang, H.; Deranlot, C.; Blume, R.; Schloegl, R.; Fert, A.; Anane, A.; Hofmann, S.; Seneor, P.; Robertson, J. Graphene-Passivated Nickel as an Oxidation-Resistant Electrode for Spintronics. *ACS Nano* **2012**, *6*, 10930–10934.

(22) Martin, M.-B.; Dlubak, B.; Weatherup, R. S.; Yang, H.; Deranlot, C.; Bouzehouane, K.; Petroff, F.; Anane, A.; Hofmann, S.; Robertson, J.; Fert, A.; Seneor, P. Sub-Nanometer Atomic Layer Deposition for Spintronics in Magnetic Tunnel Junctions Based on Graphene Spin-Filtering Membranes. *ACS Nano* **2014**, *8*, 7890–7895.

(23) Martin, M.-B.; Dlubak, B.; Weatherup, R. S.; Piquemal-Banci, M.; Yang, H.; Blume,

R.; Schloegl, R.; Collin, S.; Petroff, F.; Hofmann, S.; Robertson, J.; Anane, A.; Fert, A.; Seneor, P. Protecting Nickel with Graphene Spin-Filtering Membranes: A Single Layer Is Enough. *Appl. Phys. Lett.* **2015**, *107*, 12408.

(24)   Kumar, S.; McEvoy, N.; Kim, H.-Y.; Lee, K.; Peltekis, N.; Rezvani, E.; Nolan, H.; Weidlich, A.; Daly, R.; Duesberg, G. S. CVD Growth and Processing of Graphene for Electronic Applications. *Phys. Status Solidi B* **2011**, *248*, 2604–2608.

(25)   Britnell, L.; Gorbachev, R. V; Jalil, R.; Belle, B. D.; Schedin, F.; Katsnelson, M. I.; Eaves, L.; Morozov, S. V; Mayorov, A. S.; Peres, N. M. R.; Neto, A. H. C.; Leist, J.; Geim, A. K.; Ponomarenko, L. a; Novoselov, K. S. Electron Tunneling through Ultrathin Boron Nitride Crystalline Barriers. *Nano Lett.* **2012**, *12*, 1707–1710.

(26)   Kirczenow, G. Ideal Spin Filters: A Theoretical Study of Electron Transmission through Ordered and Disordered Interfaces between Ferromagnetic Metals and Semiconductors. *Phys. Rev. B* **2001**, *63*, 54422.

(27)   Dankert, A.; Venkata Kamalakar, M.; Wajid, A.; Patel, R. S.; Dash, S. P. Tunnel Magnetoresistance with Atomically Thin Two-Dimensional Hexagonal Boron Nitride Barriers. *Nano Res.* **2015**, *8*, 1357–1364.

(28)   Kamalakar, M. V.; Dankert, A.; Kelly, P. J.; Dash, S. P. Inversion of Spin Signal and Spin Filtering in Ferromagnet|Hexagonal Boron Nitride-Graphene van Der Waals Heterostructures. *Sci. Rep.* **2016**, *6*, 21168.

(29)   Asshoff, P. U.; Sambricio, J. L.; Rooney, A. P.; Slizovskiy, S.; Mishchenko, A.; A M Rakowski; Hill, E. W.; Geim, A. K.; Haigh, S. J.; Fal'ko, V. I.; Vera-Marun, I. J.; Grigorieva, I. V. Magnetoresistance of Vertical Co-Graphene-NiFe Junctions Controlled by Charge Transfer and Proximity-Induced Spin Splitting in Graphene. *2D Mater.* **2017**, *4*, 31004.

(30)   Gibb, A. L.; Alem, N.; Chen, J.; Erickson, K. J.; Ciston, J.; Gautam, A.; Linck, M.; Zettl, A. Atomic Resolution Imaging of Grain Boundary Defects in Monolayer. *J. Am. Chem. Soc.* **2013**, *135*, 6758–6761.

(31)   Weatherup, R. S.; Dlubak, B.; Hofmann, S. Kinetic Control of Catalytic CVD for High Quality Graphene at Low Temperatures. *ACS Nano* **2012**, *6*, 9996–10003.

(32)   Cabrero-Vilatela, A.; Weatherup, R. S.; Braeuninger-Weimer, P.; Caneva, S.; Hofmann, S. Towards a General Growth Model for Graphene CVD on Transition Metal Catalysts. *Nanoscale* **2016**, *8*, 2149–2158.

(33)   Müller, F.; Hüfner, S.; Sachdev, H.; Gsell, S.; Schreck, M. Epitaxial Growth of Hexagonal Boron Nitride Monolayers by a Three-Step Boration-Oxidation-Nitration Process. *Phys. Rev. B - Condens. Matter Mater. Phys.* **2010**, *82*, 75405.

(34)   Welsh, I. D.; Sherwood, P. M. A. Photoemission and Electronic-Structure of FeOOH - Distinguishing Between Oxide and Oxyhydroxide. *Phys. Rev. B* **1989**, *40*, 6386–6392.

(35)   Blume, R.; Kidambi, P. R.; Bayer, B. C.; Weatherup, R. S.; Wang, Z.-J.; Weinberg, G.; Willinger, M.-G.; Greiner, M.; Hofmann, S.; Knop-Gericke, A.; Schlögl, R. The Influence of Intercalated Oxygen on the Properties of Graphene on Polycrystalline Cu under Various Environmental Conditions. *Phys. Chem. Chem. Phys.* **2014**, *16*, 25989–26003.

(36)   Usachov, D.; Adamchuk, V. K.; Haberer, D.; Grüneis, A.; Sachdev, H.; Preobrajenski, A. B.; Laubschat, C.; Vyalikh, D. V. Quasifreestanding Single-Layer Hexagonal Boron

Nitride as a Substrate for Graphene Synthesis. *Phys. Rev. B* **2010**, *82*, 75415.

(37) Preobrajenski, A. B.; Vinogradov, A. S.; Mårtensson, N. Monolayer of H-BN Chemisorbed on Cu(111) and Ni(111): The Role of the Transition Metal 3d States. *Surf. Sci.* **2005**, *582*, 21–30.

(38) Nagashima, A.; Tejima, N.; Gamou, Y.; Kawai, T.; Oshima, C. Electronic Structure of Monolayer Hexagonal Boron Nitride Physisorbed on Metal Surfaces. *Phys. Rev. Lett.* **1995**, *75*, 3918–3921.

(39) Liu, N.; Pan, Z.; Fu, L.; Zhang, C.; Dai, B.; Liu, Z. The Origin of Wrinkles on Transferred Graphene. *Nano Res.* **2011**, *4*, 996–1004.

(40) Ashby, M. F.; Jones, D. R. H. Oxidation and Corrosion. In *Engineering Materials I: An Introduction to Properties, Applications, and Design*; 2012; pp 385–400.

(41) Jagadeesh, R. V.; Surkus, A.-E.; Junge, H.; Pohl, M.-M.; Radnik, J.; Rabeah, J.; Huan, H.; Schunemann, V.; Bruckner, A.; Beller, M. Nanoscale Fe2O3-Based Catalysts for Selective Hydrogenation of Nitroarenes to Anilines. *Science* **2013**, *342*, 1073–1076.

(42) Luo, W.; Zafeiratos, S. A Brief Review of the Synthesis and Catalytic Applications of Graphene-Coated Oxides. *ChemCatChem* **2017**, *2*, 2432–2442.

(43) Kravets, V. G.; Jalil, R.; Kim, Y.-J.; Ansell, D.; Aznakayeva, D. E.; Thackray, B.; Britnell, L.; Belle, B. D.; Withers, F.; Radko, I. P.; Han, Z.; Bozhevolnyi, S. I.; Novoselov, K. S.; Geim, A. K.; Grigorenko, A. N. Graphene-Protected Copper and Silver Plasmonics. *Sci. Rep.* **2014**, *4*, 5517.

(44) Grosvenor, A. P.; Kobe, B. A.; McIntyre, N. S. Examination of the Oxidation of Iron by Oxygen Using X-Ray Photoelectron Spectroscopy and QUASES. *Surf. Sci.* **2004**, *565*, 151–162.

(45) Grosvenor, A. P.; Kobe, B. A.; McIntyre, N. S. Studies of the Oxidation of Iron by Water Vapour Using X-Ray Photoelectron Spectroscopy and QUASES. *Surf. Sci.* **2004**, *572*, 217–227.

(46) Zhang, Y.; Weng, X.; Li, H.; Li, H.; Wei, M.; Xiao, J.; Liu, Z.; Chen, M.; Fu, Q.; Bao, X. Hexagonal Boron Nitride Cover on Pt(111): A New Route to Tune Molecule-Metal Interaction and Metal-Catalyzed Reactions. *Nano Lett.* **2015**, *15*, 3616–3623.

(47) Brugger, T.; Ma, H.; Iannuzzi, M.; Berner, S.; Winkler, A.; Hutter, J.; Osterwalder, J.; Greber, T. Nanotexture Switching of Single-Layer Hexagonal Boron Nitride on Rhodium by Intercalation of Hydrogen Atoms. *Angew. Chemie - Int. Ed.* **2010**, *49*, 6120–6124.

(48) Sutter, P.; Sadowski, J. T.; Sutter, E. A. Chemistry under Cover: Tuning Metal-Graphene Interaction by Reactive Intercalation. *J. Am. Chem. Soc.* **2010**, *132*, 8175–8179.

(49) Gao, J.; Li, B.; Tan, J.; Chow, P.; Lu, T. M.; Koratkar, N. Aging of Transition Metal Dichalcogenide Monolayers. *ACS Nano* **2016**, *10*, 2628–2635.

(50) Favron, A.; Gaufrès, E.; Fossard, F.; Phaneuf-L'Heureux, A.-L.; Tang, N. Y.-W.; Lévesque, P. L.; Loiseau, A.; Leonelli, R.; Francoeur, S.; Martel, R. Photooxidation and Quantum Confinement Effects in Exfoliated Black Phosphorus. *Nat. Mater.* **2015**, *14*, 826–832.

(51) Rong, Y.; He, K.; Pacios, M.; Robertson, A. W.; Bhaskaran, H.; Warner, J. H.

Controlled Preferential Oxidation of Grain Boundaries in Monolayer Tungsten Disulfide for Direct Optical Imaging. *ACS Nano* **2015**, *9*, 3695–3703.

(52) Kidambi, P. R.; Blume, R.; Kling, J.; Wagner, J. B.; Baehtz, C.; Weatherup, R. S.; Schloegl, R.; Bayer, B. C.; Hofmann, S. In Situ Observations during Chemical Vapor Deposition of Hexagonal Boron Nitride on Polycrystalline Copper. *Chem. Mater.* **2014**, *26*, 6380–6392.

(53) Simonov, K. A.; Vinogradov, N. A.; Ng, M. L.; Vinogradov, A. S.; Mårtensson, N.; Preobrajenski, A. B. Controllable Oxidation of H-BN Monolayer on Ir(111) Studied by Core-Level Spectroscopies. *Surf. Sci.* **2012**, *606*, 564–570.

(54) Galbiati, M.; Stoot, A. C.; Mackenzie, D. M. A.; Bøggild, P.; Camilli, L. Real-Time Oxide Evolution of Copper Protected by Graphene and Boron Nitride Barriers. *Sci. Rep.* **2017**, *7*, 39770.

(55) Shen, L.; Zhao, Y.; Wanf, Y.; Song, R.; Yao, Q.; Chen, S.; Chai, Y. Long-Term Corrosion Barrier with Insulating Boron Nitride Monolayer. *J. Mater. Chem. A* **2016**, *4*, 5044–5050.

(56) Li, X.; Yin, J.; Zhou, J.; Guo, W. Large Area Hexagonal Boron Nitride Monolayer as Efficient Atomically Thick Insulating Coating against Friction and Oxidation. *Nanotechnology* **2014**, *25*, 105701.

(57) Schriver, M.; Regan, W.; Gannett, W. J.; Zaniewski, A. M.; Crommie, M. F.; Zettl, A. Graphene as a Long-Term Metal Oxidation Barrier: Worse than Nothing. *ACS Nano* **2013**, *7*, 5763–5768.

(58) Dlubak, B.; Kidambi, P. R.; Weatherup, R. S.; Hofmann, S.; Robertson, J. Substrate-Assisted Nucleation of Ultra-Thin Dielectric Layers on Graphene by Atomic Layer Deposition. *Appl. Phys. Lett.* **2012**, *100*, 173113.

(59) Gao, L.; Ren, W.; Xu, H.; Jin, L.; Wang, Z.; Ma, T.; Ma, L.-P.; Zhang, Z.; Fu, Q.; Peng, L.-M.; Bao, X.; Cheng, H.-M. Repeated Growth and Bubbling Transfer of Graphene with Millimetre-Size Single-Crystal Grains Using Platinum. *Nat. Commun.* **2012**, *3*, 699.

(60) Spizzirri, P. G.; Rubanov, S.; Gauja, E.; Prawer, S. Nano-Raman Spectroscopy of Silicon Surfaces. *Mater. Forum* **2008**, *32*, 161–166.
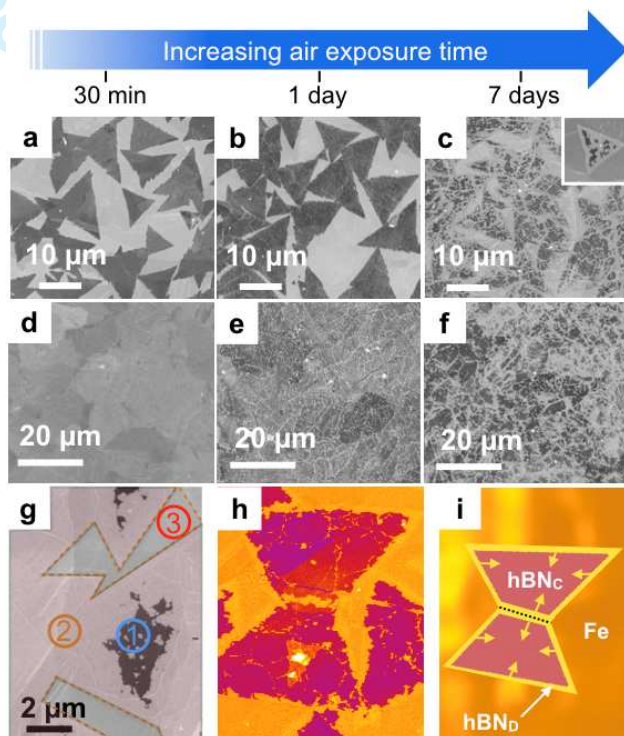
Figures

Figure 1. (a,b,c) h-BN domains on the Fe substrate after 30 min, 1 day, and 7 days of air exposure respectively. **(d,e,f)** h-BN film on the Fe substrate after 30 min, 1 day, and 7 days of air exposure respectively. The h-BN was grown at ~900 °C, by $B_3N_3H_6$ (6×10^{-4} mbar) exposure for 45 s (domains) or 12 min (films). **(g)** Detail of merging h-BN domains (left, right and top) after 7 days air exposure, illustrating a contrast difference between the middle of the domains (black, region 1), domain edges (light grey, region 2) and the uncovered Fe catalyst (dark grey, region 3). **(h)** False colour SEM image showing the detail of bow tie shaped h-BN domains after 1 day of air exposure and **(i)** corresponding schematic indicating that the change of contrast initiates at the domain edges and domain boundaries (dotted line) and proceeds inwards. h-BN/Fe_M and h-BN/Fe_{OX} indicate h-BN covering metallic and oxidized Fe regions respectively.
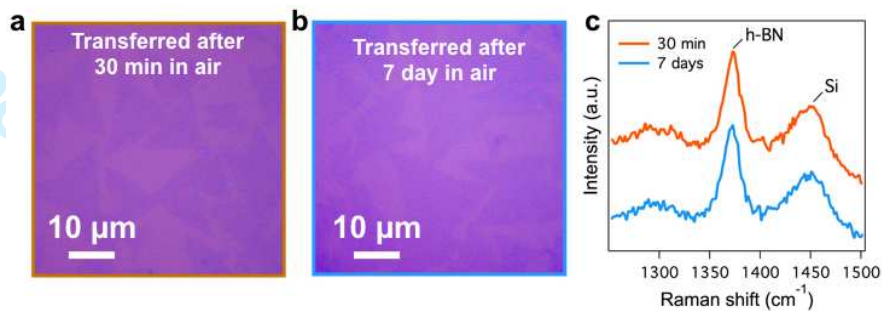
Figure 2. Optical images after transfer onto SiO_2(300 nm)/Si of **(a)** fresh h-BN domains (transferred directly after growth), **(b)** h-BN domain exposed to air 7 days and then transferred, showing that the triangular shape and size is preserved for both air exposure times. **(c)** Raman spectra of the samples in (a) and (b) displaying the characteristic peak of h-BN at ~1370 cm^{-1} and the Si substrate-related peak.[60]
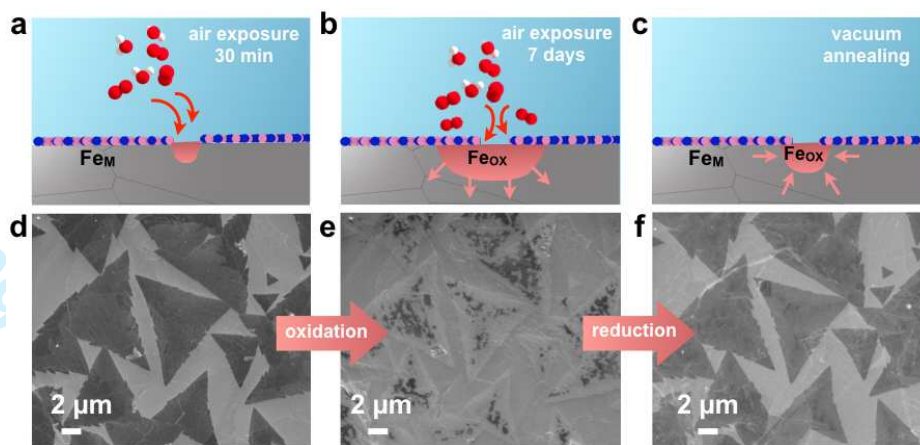
25

Figure 3. Schematics illustrating **(a)** single layer h-BN on Fe foil after a short air exposure, showing initial traces of Fe oxidation, close to h-BN defect sites or domain edges (pink area), **(b)** the same h-BN sample after 7 days in air, showing gradual oxidation of the Fe through the catalyst bulk and **(c)** reduction of the Fe during annealing in vacuum at ~600 °C for 1 hour. **(d,e,f)** Corresponding SEM images of the samples described in (a,b,c) showing a fresh sample (30 min air exposure), the same sample after 7 days air exposure, and again following vacuum annealing.
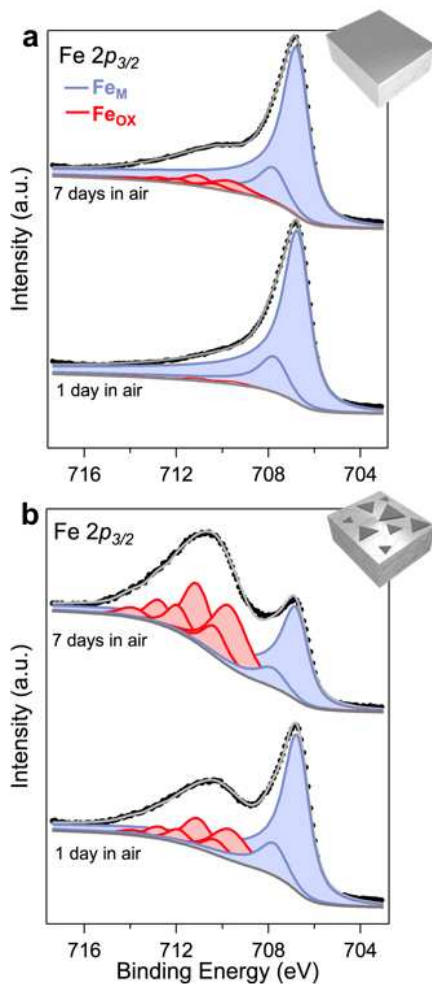
Figure 4. XP spectra of the Fe $2p_{3/2}$ core level for **(a)** a continuous single layer h-BN film and **(b)** discontinuous single layer h-BN domains as a function of air exposure time (1 day and 7 days). We note that the level of oxidation in (b) does not imply that the domains do not protect the Fe, as the spectra are acquired from a ~150 μm^2 area of the sample which includes both h-BN covered and uncovered regions. The spectra are collected at a photon energy, E_{photon}, of 1486.6 eV.
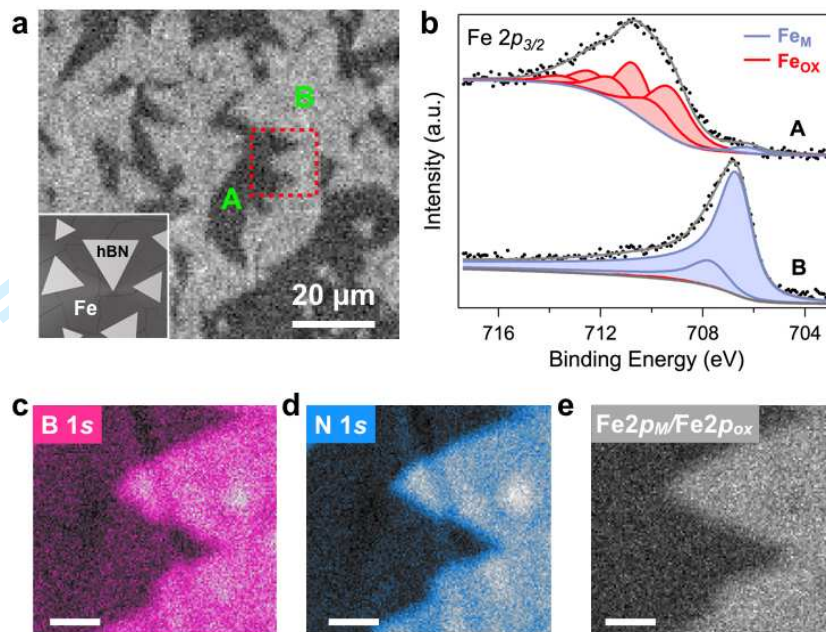
Figure 5. (a) Scanning photoemission spectroscopy (SPEM) map using the B 1*s* core level energy, showing h-BN domains grown on Fe foil [~900 °C, $B_3N_3H_6$ (6×10^{-4} mbar) for 45 s, air exposed for ~40 hours]. Inset: schematic illustrating that the light grey triangles correspond to single layer h-BN and the surrounding dark regions correspond to the bare Fe surface. **(b)** Micro-focussed XP spectra of the Fe $2p_{3/2}$ core level acquired on the bare Fe (region A) and on an h-BN domain (region B). SPEM map of the tips and edges of several h-BN domains from the region within the red dotted box acquired with **(c)** B 1*s* and **(d)** N 1*s* core level energies, and **(e)** chemical information without topography of the Fe $2p_{3/2}$ metal/oxide peak area ratio. The scalebars in c-e are 2 μm. The Fe $2p_{3/2}$, B 1*s* and N 1*s* spectra are collected at a photon energy, E_{photon}, of 1102 eV.

Table of Contents Figure
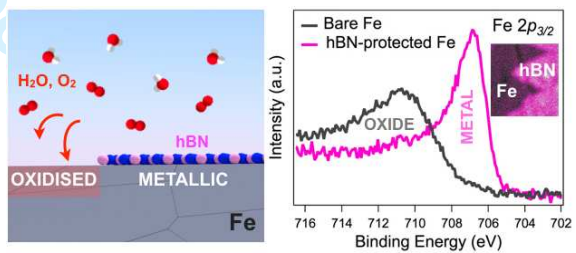
From growth surface to device interface: preserving metallic Fe under monolayer hexagonal boron nitride

Caneva, Sabina